NeuroImage: Clinical 24 (2019) 102058

Contents lists available at ScienceDirect

NeuroImage: Clinical

journal homepage: www.elsevier.com/locate/ynicl

Brain iron content in systemic iron overload: A beta-thalassemia quantitative MRI study

Renzo Manara[a], Sara Ponticorvo[a], Immacolata Tartaglione[b], Gianluca Femina[a], Andrea Elefante[c], Camilla Russo[c], Pasquale Alessandro Carafa[d], Mario Cirillo[e], Maddalena Casale[b], Angela Ciancio[f], Rosanna Di Concilio[g], Elisa De Michele[h], Nikolaus Weiskopf[i], Francesco Di Salle[a,j], Silverio Perrotta[*,b], Fabrizio Esposito[a,j]

[a] Department of Medicine, Surgery and Dentistry, Scuola Medica Salernitana, University of Salerno, Baronissi, Salerno 84081, Italy
[b] Department of Woman, Child and Specialist Surgery, Università della Campania "Luigi Vanvitelli", Napoli 80138, Italy
[c] Neuroradiologia, Università degli Studi di Napoli "Federico II", Napoli, Italy
[d] Dipartimento di Salute Mentale e Fisica e Medicina Preventiva, Università della Campania "Luigi Vanvitelli", Napoli, Italy
[e] Dipartimento di Scienze Mediche, Chirurgiche, Neurologiche, Metaboliche e dell'Invecchiamento, Università della Campania "Luigi Vanvitelli", Napoli, Italy
[f] Unità Operativa Ematologia - Day Hospital di Talassemia, Ospedale "Madonna delle Grazie", Matera, Italy
[g] Dipartimento di Pediatria, Ospedale "Umberto I", Nocera Inferiore, Italy
[h] Medicina Trasfusionale AUO "San Giovanni di Dio e Ruggi D'Aragona", Salerno, Italy
[i] Department of Neurophysics, Max Planck Institute for Human Cognitive and Brain Sciences, Leipzig, Germany
[j] Department of Diagnostic Imaging, University Hospital "San Giovanni di Dio e Ruggi d'Aragona", Scuola Medica Salernitana, Salerno 84131, Italy

ARTICLE INFO

Keywords:
Beta-thalassemia
Brain MRI
Multi-parametric mapping
Iron
Blood transfusion

ABSTRACT

Objective: Multisystem iron poisoning is a major concern for long-term beta-thalassemia management. Quantitative MRI-based techniques routinely show iron overload in heart, liver, endocrine glands and kidneys. However, data on the brain are conflicting and monitoring of brain iron content is still matter of debate.
Methods: This 3T-MRI study applied a well validated high-resolution whole-brain quantitative MRI assessment of iron content on 47 transfusion-dependent (mean-age: 36.9 ± 10.3 years, 63% females), 23 non-transfusion dependent (mean-age: 29.2 ± 11.7 years, 56% females) and 57 healthy controls (mean-age: 33.9 ± 10.8 years, 65% females). Clinical data, Wechsler Adult Intelligence Scale scores and treatment regimens were recorded. Beside whole-brain R2* analyses, regional R2*-values were extracted in putamen, globus pallidum, caudate nucleus, thalamus and red nucleus; hippocampal volumes were also determined.
Results: Regional analyses yielded no significant differences between patients and controls, except in those treated with deferiprone that showed lower R2*-values ($p < 0.05$). Whole-brain analyses of R2*-maps revealed strong age-R2* correlations ($r^2 = 0.51$) in both groups and clusters of significantly increased R2*-values in beta-thalassemia patients in the hippocampal formations and around the Luschka foramina; transfusion treatment was associated with additional R2* increase in dorsal thalami. Hippocampal formation R2*-values did not correlate with hippocampal volume; hippocampal volume did not differ between patients and controls. All regions with increased R2*-values shared a strict anatomical contiguity with choroid plexuses suggesting a blooming effect as the likely cause of R2* increase, in agreement with the available histopathologic literature evidence.
Conclusion: According to our MRI findings and the available histopathologic literature evidence, concerns about neural tissue iron overload in beta-thalassemia appear to be unjustified.

Introduction

Beta-thalassemia is a group of disorders caused by defective production in beta-globin chains of hemoglobin, determining ineffective erythropoiesis and microcytic anemia. The clinical phenotype may vary greatly, thus requiring different types of care (Taher et al.,

These authors equally contributed to the study and should be considered first coauthors.
* Corresponding author.
E-mail address: silverio.perrotta@unicampania.it (S. Perrotta).

https://doi.org/10.1016/j.nicl.2019.102058
Received 18 April 2019; Received in revised form 15 October 2019; Accepted 23 October 2019
Available online 25 October 2019

2018). The most severe form necessitates regular red blood cell transfusions since the first years of life, while less severe forms may require only occasional transfusions to face specific needs (e.g. during growth, pregnancy or infections). While chronic anemia has achieved a good control, at least where regular blood treatment is available, multisystem involvement during the disease course occurs in almost all clinical phenotypes because of systemic iron overload. The latter derives not only from blood transfusion regimens but also from ineffective erythropoiesis and increased gastrointestinal absorption, approximately 3 to 4 times greater than normal (Gardenghi et al., 2007). Each unit of packed red blood cells contains approximately 200–250 mg of iron (Á et al., 2013) that largely overwhelms iron excretion capabilities (about 1 mg/day) (Hunt et al., 2009) thus heavily concurring to persistently high serum ferritin levels and multiorgan iron poisoning. Detecting iron overload before overt organ damage allows a tailored chelation therapy that helps to prevent organ failure or to revert early stages of iron-related comorbidities (Anderson et al., 2004; Casale et al., 2014). Iron monitoring is therefore crucial and usually rely on serum ferritin levels, albeit these do not strictly correlate with tissue iron accumulation (Aubart et al., 2016) in all organs. Direct measurement of iron stores is only achievable through biopsy (e.g. liver biopsy), which cannot be easily or repeatedly obtained for all organs (Ambu et al., 1995).

In the last two decades, quantitative MRI-based techniques have allowed a precious in vivo non-invasive assessment of iron stores at least for the most vulnerable organs (e.g. heart and liver). Indeed, cardiac and liver T2* MRIs are now part of the routine management of beta-thalassemia (Viprakasit et al., 2018). In recent years, the same approach has been applied for endocrine glands, pituitary gland included, and kidneys, helping to better characterize the iron-related multisystem involvement (Bozdağ et al., 2017; Hashemieh et al., 2017; Kosaryan et al., 2017).

Recent methodological advances have provided in vivo brain iron content quantification via MRI mapping of the effective transverse relaxation rate ($R2^* = 1/T2^*[s^{-1}]$). This approach has been previously validated for the brain with histological measurements (Langkammer et al., 2010) and can be boosted using multiple three-dimensional pulse sequences in reasonable scan time (Deoni et al., 2005; Dick et al., 2012; Helms and Dechent, 2009; Sereno et al., 2013) at clinical magnetic field strength (1.5–3.0 Tesla). Particularly, a multi-parametric mapping acquisition protocol based on multi-echo 3D Fast Low-Angle Shot (FLASH) sequences has been recently well validated to obtain high resolution (≤ 1 mm) whole brain maps of iron content via voxel-based quantification of R2* parameters (Helms et al., 2008, 2008; Weiskopf et al., 2011, 2014). The multi-parametric mapping protocol provides standardized metrics with a high degree of reproducibility (Weiskopf et al., 2013) and enables the extraction of iron deposition patterns in large cohorts without the need of a priori localization and tailoring of the regions of interest (Whitaker et al., 2016; Callaghan et al., 2014).

In the attempt to solve the question if brain iron overload is real in beta-thalassemia, here we performed a voxel-based whole-brain quantitative MRI study of iron content involving 70 beta-thalassemia patients (recruited from 4 major centers in Southern Italy) and 57 age and sex matched controls to compare iron (R2*) brain maps between transfusion dependent/non transfusion dependent beta-thalassemia patients and controls without prior assumptions on the potential sites of aberrant iron accumulations.

Material and method

Subjects

Transfusion-dependent and non-transfusion-dependent patients were recruited from 4 referral centers for beta-thalassemia. Inclusion criteria were: diagnosis of beta-thalassemia and age >16 years. Patients were considered with Transfusion Dependent Thalassemia (TDT) if on a regular transfusion regimen over the last 10 years; those who were not regularly transfused and had not received any transfusion during the last 48 weeks before the enrolment were enrolled as subjects with Non Transfusion Dependent Thalassemia (NTDT).

Exclusion criteria were contraindications to MRI, history of neurologic disease, head trauma or neurosurgery. Controls were healthy volunteers aged >16 years mostly recruited among patients' relatives and entourage.

A clinical chart review allowed the collection of clinical and laboratory data related to the disease history and severity; laboratory parameters were collected as mean of last year's values. All data were acquired between June 2016 and June 2017. Patients and healthy subjects also participated to studies on cerebrovascular involvement (Tartaglione et al., 2019) and on cognitive involvement. (Tartaglione et al., 2019)

The study protocol was approved by the institutional review board and written informed consent was obtained from each participant according to the Declaration of Helsinki.

Neurological and cognitive evaluation

All subjects were briefly evaluated before brain MRI: gait, coordination, speech, motor strength, main cranial nerves were assessed and a rapid clinical interview investigated previous history of neurological dysfunction. Neurological impairment was an exclusion criterion. Most study subjects (66/74 patients and 45/56 healthy controls) underwent Intelligence Quotient (IQ) testing using the Wechsler Adult Intelligence Scale-Fourth Edition (WAIS-IV)

Quantitative MRI

Whole brain data were acquired on the same 3T MRI scanner (MAGNETOM Skyra, Siemens, Erlangen Germany) with a 20-channel head coil. The qMRI imaging protocol consisted of three multi-echo 3D FLASH sequences according to the multi-parametric mapping protocol (Weiskopf and Helms, 2008), respectively with predominant T1-, proton density-, and Magnetization Transfer-weighting (more details Supplemental file 1). All the multi-parametric mapping sequences were acquired at 1 mm isotropic resolution. In addition to the multi-parametric mapping series, a 3D T1-weighted magnetization prepared rapid gradient echo (MPRAGE) sequence (repetition-time = 2400 ms, echo-time = 2.25 ms, resolution = $1 \times 1 \times 1$ mm (Á et al., 2013), matrix-size = 256×256, anterior-posterior phase encoding direction, generalized autocalibrating partially parallel acquisition (GRAPPA) factor of 2 in phase-encoding direction) was also acquired for volumetric analyses. The scan time was 26 min for each subject.

Iron content analysis

Quantitative whole brain R2* maps were estimated using SPM12 (www.fil.ion. ucl.ac.uk/spm) running on Matlab R2014a (The MathWorks Inc., Natick, MA, USA) and the voxel-based quantification batch tool (Draganski et al., 2011). The R2* value at each voxel was estimated with the ESTATICS (estimating the apparent transverse relaxation time R2* from images with different contrasts) method which is based on a linear regression on the logarithm of the signal intensities of all echo images of all multi-parametric mapping series (PD, T1 and MT multi-echo images) (Weiskopf et al., 2014). The Signal to Noise (SNR) ratio was calculated as the ratio between the mean signal intensity in the brain and the standard deviation of the noise in each echo time for each contrast, to estimate the quality of the original acquired images, and the root-mean-square error, was quantified at each voxel to evaluate the goodness of the parameter fitting.

For the voxel-based quantification analysis, the Magnetization Transfer maps were segmented into gray matter and white matter probability maps using the unified segmentation approach

Table 1
Subjects baseline characteristics.

		All patients	TDT	NTDT	HC
# of patients		70	47	23	57
Females, n (%)		43 (61)	30 (63)	13 (56)	37(65)
Age (years), mean ± SD median (range) IQR		34.4 ± 10.8 34 (16–65) 17.5	36.9 ± 10.3 39 (16–65) 17	29.2 ± 11.7 26 (16–52) 14.5	39.9 ± 10.8 32 (17–66) 14.2
Age at first transfusion (months), mean ± SD median (range) IQR		29 ± 42.5 24 (2–276) 30	29 ± 42.5 24 (2–276) 30	n.a.	n.a.
Splenectomy, n (%)		46 (66)	37 (79)	9 (39)	0(0)
Hb (g/dl), mean ± SD median (range)IQR		9.3 ± 1.0 9.3 (7.4–10.8) 1.4	9.3 ± 0.9 9.3 (7.4–10.8) 1.2	9.3 ± 0.9 9.8 (8.1–10.8) 1.4	n.a.
Transfusion Index (ml/kg/year) median (range) IQR		149.9 ± 55.1 143 (60–288) 67	149.9 ± 55.1 143 (60–288) 67	0	0
Ferritin (ng/ml), mean ± SD median (range) IQR		729.1 ± 628.0 500 (75–2314) 614	882.8 ± 669.0 714.5 (140–2314) 637	364.1 ± 290.8 280 (75–1000) 294.5	n.a.
HCV+, n (%)		7 (10.0)	7 (14.9)	0	0
LIC (mg/gdw), mean ± SD median (range) IQR		4.9 ± 3.7 3.7 (1–20.5) 5.1	4.4 ± 3.1 3.5 (1–13.7) 3.7	6.7 ± 5.4 6.35 (1–20.5) 7.65	n.a.
Heart T2*(msec), mean ± SD median (range) IQR		32.5 ± 15.7 31.9 (13.1–65.9) 14.2	31.9 ± 11.3 32 (13.1–65.9) 12.4	34.6 ± 20.3 29.5 (15.9–55.3) 18.5	n.a.
ICT	DFO ever, n (%) ongoing, n (%) dose, mg/kg	51 (72.8) 13 (18.6) 33.5 ± 6.7	46 (97.9) 11 (23) 35.9 ± 3.1	5 (21.7) 2 (8.7) 20.0 ± 1.6	0
	DFP ever, n (%) ongoing, n (%) dose, mg/kg	20 (28.6) 3 (4.3) 72.9 ± 1.8	19 (40.4) 2 (4.2) 73.2 ± 2.5	1 (4.3) 1 (4.3) 72.4	0
	DFX ever, n (%) ongoing, n (%) dose, mg/kg	53 (75.7) 35 (50.0) 21.5 ± 10.7	45 (95.7) 32 (71.1) 27.6 ± 8.0	8 (34.8) 3 (13) 10.1 ± 0.6	0

Table 1. Characterization of the patients and controls enrolled. LIC: liver iron concentration; ICT: iron chelation therapy; DFO: deferoxamine; DFP: deferiprone; DFX: deferasirox dispersible tablets; IQR: interquartile range.

(Ashburner and Friston, 2005) and the inter-subject registration (normalization) was performed with the non-linear diffeomorphic algorithm DARTEL (Ashburner, 2007). DARTEL normalization was then applied to all iron-related (R2*) maps in combination with tissue-specific probability weighting and isotropic Gaussian smoothing (3 mm full width half maximum), as previously described (Draganski et al., 2011). Besides DARTEL, a combined volumetric and surface normalization (Postelnicu et al., 2009) was also applied to multi-parametric mapping images to perform a different voxel-based quantification analysis without tissue-specific probability weighting (and masking) and without smoothing (Canna et al., 2018; Maldjian et al., 2003).

The hippocampal volume was calculated from the MPRAGE images using the automated Freesurfer (https://surfer.nmr.mgh.harvard.edu/) total reconstruction pipeline which consents the whole-brain segmentation in a single-subject basis and the consequent extraction of several structural brain metrics.

Statistical analysis

The between-group statistical comparisons of iron-related maps were performed in SPM12 by fitting an analysis of covariance (ANCOVA) linear model including age, sex and total intra-cranial volume of the subjects as covariates and running multiple post-hoc t-tests on the fitted parameters, over all gray matter voxels. For the voxel-based analysis a gray matter mask was used as previously suggested (Callaghan et al., 2014) and family-wise error corrections for multiple comparisons were applied using gaussian random field theory as implemented in SPM12.

In addition to the voxel-based analysis, regional R2* values were extracted for each participant in a priori regions of interest (ROIs) defined in the putamen, globus pallidum, caudate nucleus and thalamus, using the Harvard-Oxford subcortical standard atlas (https://fsl.fmrib.ox.ac.uk/fsl/fslwiki/Atlases), and in red nucleus using the PickAtlas Matlab toolbox (Postelnicu et al., 2009). ROI mean values were compared between groups and linearly correlated with age in the three groups of subjects. A posteriori ROIs were also defined based on the results of the voxel-based analyses.

ROI-based ANCOVA analyses were also performed, and Pearson's correlation coefficients were calculated, to respectively investigate the differences in R2* values in relation to splenectomy and chelation treatment including deferiprone (ongoing or previous treatment, three and twenty-three TDT patients, respectively), and the correlation between R2* values and subjects' age in all groups and structural (hippocampal volume), and clinical (serum ferritin levels and LIC) findings among patients. The analysis of cognitive data was restricted to the patients for whom the data were available (i.e. missing cognitive data were not extrapolated). Statistical thresholds were applied at $p = 0.05$ after correction for multiple comparisons using the Bonferroni method.

Data availability statement

Individual de-identified participant imaging data in DICOM format will be shared upon request from other investigators for purposes of replicating procedures and results. De-identified clinical and pre-processed imaging data in NIFTI format, as well as accompanying documents describing the study protocol and the detailed procedures (software codes) used in the statistical analysis, will be also shared upon request from any qualified investigator.

All requests should be sent via email to the corresponding author who will provide within three weeks a web link to a trusted data repository together with detailed information for secure (password-protected) log-in and secure download of the data from the repository.

Results

Among 152 adult beta-thalassemia patients followed in the participating sites 11 were excluded due to one of the exclusion criteria listed above: contraindications to MRI (1 patient with implantable cardioverter defibrillator, 6 with claustrophobia), history of head trauma (1), history of neurologic disease (1 perinatal hypoxic ischemic encephalopathy, 1 congenital viral infection, 1 stroke). Among the remaining 141 beta-thalassemia patients (all neurologically asymptomatic and potentially recruitable), 62 did not participate because of poor compliance (mostly because of excessive distance from the center where MR-examinations were performed), 7 had excessive motion artifacts and 2 interrupted prematurely the exam.

Forty-seven transfusion dependent patients (TDT; mean-age: 36.9 ± 10.3 years, 63% females), 23 non-transfusion dependent patients (NTDT; mean-age: 29.2 ± 11.7 years, 56% females) and 57 healthy controls (HC; age: 33.9 ± 10.8 years, 65% females) were enrolled in the study. Patients subgroups and controls did not differ for age and gender ($p > 0.5$).

The main demographic and clinical characteristics of the beta-thalassemia patients and controls are shown in Table 1. No patient or control showed overt or silent territorial, hemodynamic or lacunar stroke. Nineteen patients had history of HCV: 12/19 cleared after therapy in 2015–2016. Serum ferritin levels of the 7/19 HCV+ TDT patients did not differ from those observed in HCV- TDT patients.

Psychometrics

The overall assessment of cognitive function showed lower IQ values in beta-thalassemia patients compared to controls (76.0 ± 19.3 versus 97.8 ± 18.1 $p < 0.0001$). The differences persisted after correction for education level. IQ values did not correlate with age and showed no significant sex-related differences.

ROI-based analysis of iron-related (R2) maps*

In all a priori selected gray matter subcortical ROIs (putamen, globus pallidum, caudate nucleus, thalamus, red nucleus) no significant differences were found in the R2* values between TDT and NTDT patient subgroups ($p > 0.05$, with or without correction for multiple comparisons, see Table 2). In addition, no association was found between regional R2* values and splenectomy, and no significant correlation was found with LIC values. Only the three patients under ongoing chelation therapy with deferiprone showed lower-than-average R2* values (Supplemental Figure 1). However, patients with a previous history of deferiprone treatment (sixteen TDT patients in total, after excluding the three patients with ongoing deferiprone treatment) did not show significantly decreased R2* values compared to controls or to patients who had never had deferiprone treatment. The slopes of the estimated linear correlation between mean regional R2* values and age are reported in Table 3 separately for each group.

Table 2
Mean ± standard deviation of R2* values [s^{-1}] across subjects.

	HC [s^{-1}]		NTDT [s^{-1}]		TDT [s^{-1}]	
Left CN	16.86	± 1.58	16.59	± 1.43	16.10	± 1.68
Right CN	16.31	± 1.79	15.92	± 1.31	15.59	± 1.66
Left Put	15.10	± 1.84	15.86	± 1.85	15.49	± 2.60
Right Put	15.08	± 2.05	15.49	± 1.73	15.33	± 2.84
Left GP	19.74	± 2.30	20.57	± 2.53	20.73	± 3.29
Right GP	21.06	± 2.48	21.89	± 2.25	21.97	± 3.59
Left Thal	9.82	± 0.69	9.91	± 0.79	10.16	± 1.05
Right Thal	10.21	± 0.75	10.31	± 0.85	10.63	± 1.15
RN	20.16	± 2.21	21.29	± 2.25	21.21	± 2.78

Table 2. Mean ± standard deviation of R2 values [s^{-1}] across subjects in the three groups in the bilateral subcortical region of interest (Caudate Nucleus (CN), Putamen (Put), Globus Pallidum (GP), Thalamus (Thal) and Red Nucleus (RN)) after regressing out the variability due to subject's age and sex.*

Table 3
Slopes of linear correlation of R2* vs age.

	HC	NTDT	TDT
Left CN	0.100	0.102	0.084
Right CN	0.046	0.139	0.161
Left Put	0.178	0.234	0.138
Right Put	0.005	0.048	0.031
Left GP	0.116	0.209	0.172
Right GP	0.088	0.099	0.077
Left Thal	0.074	0.141	0.157
Right Thal	0.182	0.228	0.146
RN	0.009	0.048	0.030

Table 3. Slopes of the linear fitting of the R2 mean regional values on subject's age, separately for each group. Subcortical region of interest considered: Caudate Nucleus (CN), Putamen (Put), Globus Pallidum (GP), Thalamus (Thal) and Red Nucleus (RN).*

Whole-brain analysis of iron-related (R2) maps*

The whole-brain voxel-based analysis of R2* parameter highlighted a strong linear correlation with age ($r^2 = 0.51$; $p < 0.05$ family-wise corrected for multiple comparisons) in deep subcortical structures, and particularly in the putamina, both in controls and beta-thalassemia patients (Fig. 1).

Compared to controls, the whole group of beta thalassemia patients showed significantly higher R2* values in small symmetric clusters in the anterior hippocampal formation and around the Luschka foramina (i.e. posterior margin of the inferior cerebellar peduncle and anterior margin of the cerebellar tonsils) ($p < 0.05$ family-wise corrected for multiple comparisons; Fig. 2a, Table 4). Comparing TDT subgroup and controls, the R2* increase was even more evident with additional symmetric clusters of difference appearing in the dorsal thalamic surfaces ($p < 0.05$ family-wise corrected for multiple comparisons; Fig. 2b). No significant differences were found between NTDT patients and controls or between NTDT and TDT subgroups.

The whole-brain voxel-based analysis of R2* parameter restricted to the whole group of beta thalassemia patients did not reveal any significant correlation with serum ferritin levels over the entire gray matter. Nonetheless, some positive linear correlations were descriptively observed in two bilateral clusters ($p < 0.001$, uncorrected), which were overlapping with previous ROIs in anterior hippocampal formation, albeit located more towards the border of the gray matter, adjacent to the choroid plexuses (Fig. 3).

A separate voxel-based quantification analysis of R2* maps was also performed using combined volumetric and surface normalization instead of DARTEL normalization. This alternative normalization procedure did not include smoothing or masking of the ventricles harboring the choroid plexuses and showed that iron accumulation was unambiguously confined in the choroid plexuses (see Supplemental Figure 2).

The SNR was calculated for each echo of the MPM acquisitions and it is shown for one representative healthy subject in the supplementary figure 3(a). In general, higher SNR values were found in PD images (min to max) 2.8 to 4.1, than in MT, 1.8 to 2.9 and T1 1.6 to 2.7 images. To evaluate the resulting errors in R2* quantification, the root-mean-square error from the fitting procedure across all voxels is shown in the supplementary figure 3(b). The mean (± sd) root-mean-square error in the gray and white matter was 0.05 (± 0.06) and 0.038 (± 0.02) respectively.

Iron-related (R2) maps, serum ferritin levels, cognitive assessment scores and hippocampal formation volume*

No significant correlation was found between R2* values of "a priori" above-mentioned selected ROIs, or significant clusters from the voxel-based analysis, and the cognitive assessment scores. All clusters of

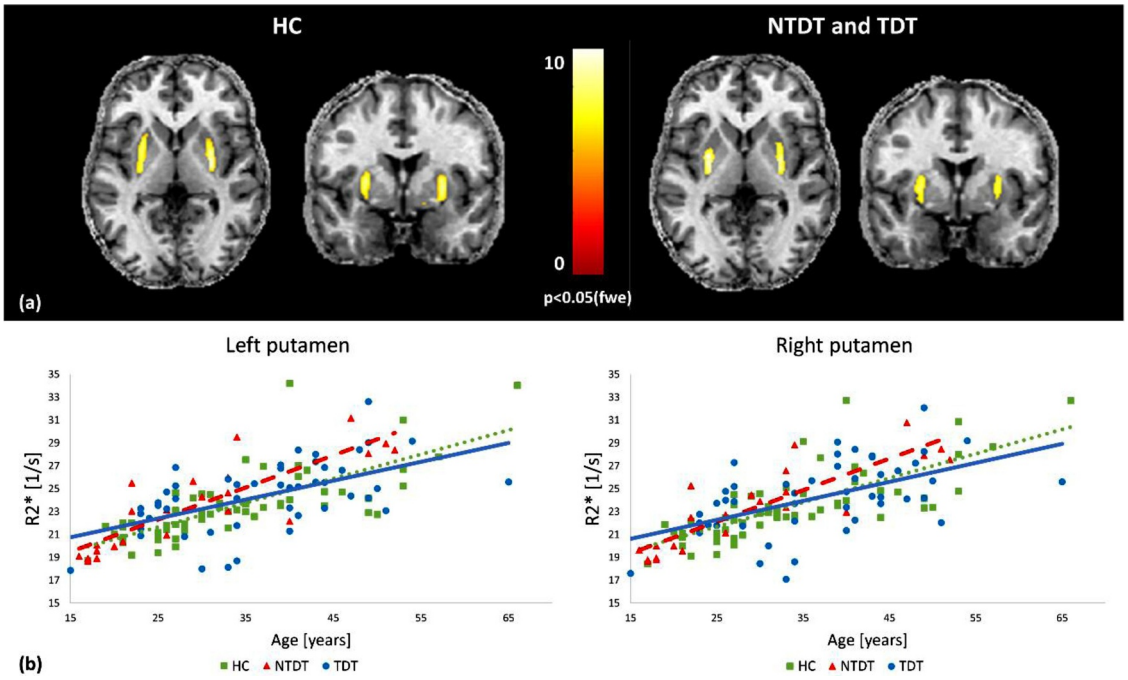

Fig. 1. (a)Whole-brain correlation maps ($p < 0.05$, family-wise error correction for multiple comparisons) of R2* vs. age in healthy subjects (left) and beta-thalassemia patients (right). (b) Scatter plot and linear trends of R2* values vs. age in the significant clusters of the bilateral putamina.

increased R2* values showed significant correlations with serum ferritin levels. Hippocampal formation R2* values showed no correlations with hippocampal volume; no significant differences were found comparing the bilateral hippocampal volume between HC and both TDT and NTDT.

Discussion

The present quantitative MRI study on beta-thalassemia patients identified a disease-related increase of iron content, only in small symmetric structures. This increase was accentuated by regular blood transfusion treatment. Nonetheless, altogether, the regional pattern of brain iron accumulation outside the neural tissue and the relationships with clinical and laboratory measures allowed interesting considerations regarding iron-related brain involvement in beta-thalassemia that will be discussed in the following sections.

Iron overload in the brain

So far, it has not been clarified whether or not the brain is a target site for aberrant iron accumulation in beta-thalassemia. Iron accumulation is a well-defined phenomenon in aging brain (Callaghan et al., 2014; Draganski et al., 2011), chronic neural tissue inflammation (Gillen et al., 2018), secondary neurodegeneration (Kuchcinski et al., 2017) or genetically determined neurodegenerative diseases (Di Meo and Tiranti, 2018) and it is associated with functional impairment in non-thalassemic diseases (Ji et al., 2017). Beta-thalassemia patients have been repeatedly shown to present poorer cognitive performances compared to normal subjects (Elalfy et al., 2017; Monastero et al., 2000) and have persistently high serum iron levels, raising major

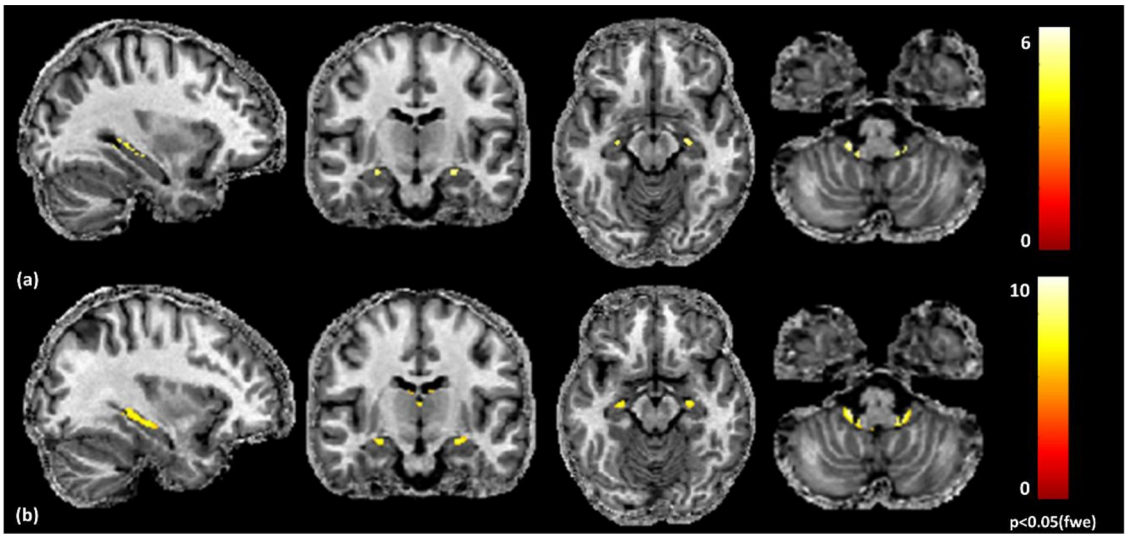

Fig. 2. T-maps of group comparison displayed on a single-subject normalized magnetization transfer (MT) map. (a) TDT and NTDT patients vs. HC. (b) TDT patients vs. HC. All maps are thresholded at $p < 0.05$ after family-wise error correction for multiple comparisons.

Table 4
Statistically significant clusters characterization.

	Cluster name	Peak coordinate (MNI)	Cluster size (voxels)
TDT and NTDT vs HC	R-LUSC	12, −43, −45	100
	L-LUSC	−15, −39, −48	90
	R-HIPP	25, −14, −15	182
	L-HIPP	−26, −16, −15	75
TDT vs HC	R-LUSC	12, −43, −46	246
	L-LUSC	−15, −38, −47	266
	R-HIPP	29, −20, −12	738
	L-HIPP	−30, −39, 0	703
	R-THAL	2, −29, 8	83
	L-THAL	−8, −20, 18	64

Table 4. Characterization of the clusters where the R2 was found different between groups ($p < 0.05$ fwe corrected). No suprathreshold clusters were found comparing NTDT vs HC and comparing TDT vs NTDT. The clusters were named for an easier localization: R-LUSC and L-LUSC are the clusters around the right and left Luschka foramina, R-HIPP and L-HIPP are the right and left clusters around the anterior hippocampal formations and R-THAL and L-THAL are the clusters on the dorsal thalamic surfaces.*

concerns about a possible iron-related brain involvement, especially in later phases of disease. Metafratzi et al. (2001) were the first to investigate the brain of beta-thalassemia patients with 2D spin-echo MRI, reporting abnormally increased iron content in putamina, caudate nuclei and motor and temporal cortices. Akhlaghpoor et al. (2012), using an improved 2D fast gradient-echo sequence, reported iron abnormalities only in the caudate nuclei and thalami. Successively, the analysis was further upgraded with the use of 3D gradient-echo MRI but none of previous regions was replicated and only midbrain red nuclei and the choroid plexuses disclosed a significant increase of iron content compared to healthy controls. (Qiu et al., 2014) Finally, Hasiloglu et al. (2017) investigated intracranial iron accumulation with susceptibility weighted MRI and, albeit neglecting the brain tissue and focusing solely on the choroid plexuses, they showed an increased iron content in transfusion-dependent patients that was linearly dependent to ferritin serum levels. These largely contradictory findings most likely depended on differences in sample sizes, patient characteristics and treatments, as patients were recruited in different countries and underwent different iron quantification MRI protocols. Moreover, all previous studies focused on regionally specific effects (using different criteria for region of interest definition) and none presented a whole-brain voxel-level analysis of iron content maps without a priori assumptions on the potentially involved regions. Thereby, these findings have not defined if iron overload systemically occurs in the brain tissue or it is just a plausible inference from evidence obtained in other organs and tissues.

A first key-point of the present iron content quantitative MRI study is the detection in a large healthy control sample of values strikingly consistent with the available literature, in terms of both amount and age-dependence within the deep gray matter (Callaghan et al., 2014; Pirpamer et al., 2016; Aquino et al., 2009). These findings strongly support the reliability of the quantitative MRI analysis even when applied in a clinical setting and pave the way for the subsequent discussion.

A second key-point is that beta-thalassemia patients showed almost identical findings, including and especially the strict age dependence, in almost the entire brain regardless of blood transfusion treatment. Therefore, our whole-brain voxel-based quantitative analysis points to no specific disease-related iron accumulation in most of the regions (e.g. putamen and red nuclei) that have been previously identified as significantly vulnerable to persistently increased serum ferritin levels. Actually, beta-thalassemia showed significant iron overload in small symmetric supratentorial and infratentorial brain regions. At a first glance, these findings seem to confirm that the brain is at least regionally vulnerable to abnormally elevated iron levels, likewise the liver, the heart or the endocrine glands. This perception might be reinforced by the direct correlation between iron content and transfusion regimen, where the treatment-related iron intake adds to the endogenous iron excess often in spite of an aggressive chelation treatment. Nonetheless, brain areas of significant iron overload in beta-thalassemia patients do not seem to share any developmental, metabolic or functional characteristics but a strict anatomical contiguity with the choroid plexuses. For example, the dorsal thalamic symmetric

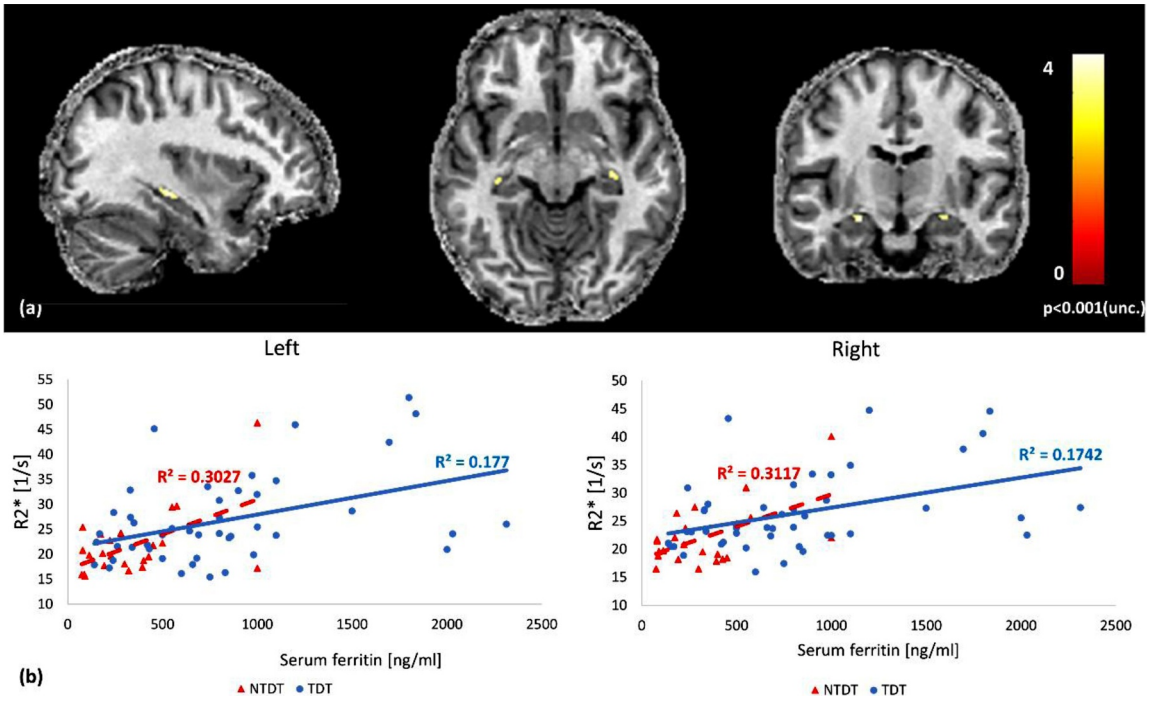

Fig. 3. (a) Whole-brain correlation maps ($p < 0.001$, uncorrected) of R2* vs. serum ferritin in both groups of beta-thalassemia patients. (b) Scatter plot, linear trends and R^2 values of R2* values vs. serum ferritin in the bilateral significant clusters.

Table 5
'A priori' region of interest-based analysis.

	Year	Patients	Age	*HC*	*Put*	*GP*	*CN*	*MC*	*TC*	*Thal*	*RN*	*ChP*
Metafratzi et al.	2001	41 TDT	24 (8.5–44)	58	+	–	+	+	+	n.e.	n.e.	n.e.
Akhlaghpoor et al.	2012	53 TM	25.9 ± 1.0	40	–	–	+	n.e.	n.e.	+	–	n.e.
Qiu et al.	2014	31 TM	25.3 ± 5.9	33	–	–	–	n.e.	n.e.	–	+	+
Hasiloglu et al.	2017	18 TDT (17 TM)	19 (7–39)*	18	n.e.	n.e.	n.e.	n.e.	n.e.	n.e.	n.e.	+
Present study	2018	47 TDT 23 NTDT	36.9 ± 10.3 29.2 ± 11.7	56	–	–	–	n.e.	n.e.-	–	–	+

*Table 5: 'A priori' region of interest-based analysis of increased iron content in the brain parenchyma: literature and present study findings. *median-age and range; TDT = transfusion dependent thalassemia; TM = thalassemia major; NTDT = not transfusion dependent thalassemia; HC = healthy controls; Put = putamen; GP = globus pallidum; CN = caudate nucleus; MC = motor cortex; TC = temporal cortex; Thal = thalamus; RN = red nucleus; ChP = choroid plexuses; + = increased iron content; - = no iron accumulation in patients; n.e. = not evaluated.*

regions identified in the comparison between TDT patients and healthy controls encompass several nuclei with different functional roles, grouped together only by the fact that the choroid plexuses of the lateral ventricles lay on them. Similarly, infratentorial regions were limited to symmetric small regions (namely the posterior aspect of the inferior cerebellar peduncles and the superficial anterior medial portion of the cerebellar tonsils) around the choroid plexuses of the IV ventricle protruding in the subarachnoid spaces through the Luschka's foramina. Finally, the most specific correlations between brain R2* values and serum ferritin levels emerged closest to the border between the gray matter and the choroid plexuses. As the choroid plexuses are known from previous studies to be highly sensitive to iron accumulation (Qiu et al., 2014; Hasiloglu et al., 2017), it is very likely that the apparent iron content increase of nearby above-mentioned regions is caused by the unavoidable smoothing implied by the volumetric normalization applied to all quantitative R2* maps for the voxel-based morphometric analysis.

More puzzling is the interpretation of iron overload within part of the hippocampal formations. These regions share indeed common embryological origin, development path, cortical structure, metabolic demand and are homogeneously committed in a few brain functions such as memory-related cognitive processes. As beta-thalassemia patients often present with significantly increased rate of impaired cognitive performances (Elalfy et al., 2017) and memory seems to be also involved (Monastero et al., 2000), the hypothesis of a selective hippocampal formation involvement appears intriguing. At the same time, along the entire superior-medial border of the hippocampal formation runs a choroid plexus raising the suspicion of a possible artifactual nature of the iron content increase. The latter hypothesis is supported by the following facts: 1) the known direct correlation between blood and choroid plexus iron levels, 2) the close anatomical adjacency between choroid plexuses and all the supratentorial and infratentorial regions, 3) the lack of atrophy of the hippocampal formation even in the more severe form of beta-thalassemia patients. On the other hand, even the ascertained artifactual origin of the measurements does not exclude the presence of a concomitant underlying iron overload in (part of) the highlighted brain regions. As a matter of fact, according to our study it is only possible to state that there is no evidence of increased iron content in the neural tissue of the brain of beta-thalassemia patients (regardless to transfusion treatment) and iron-related blooming artifacts due to plexuses overload are by far the best explanation of the above-mentioned abnormal imaging findings. Only direct pathologic investigations of these regions could be able to state the lack of iron accumulation in brain tissues but the plexuses. As far as we know, the only histopathology study describing iron content in the brain of five TDT patients (Witzleben and Wyatt, 1961) reported as follows: "*Central nervous system. No stainable and very little chemical iron is present in the parenchyma. Intense accumulations are present in the epithelium of the choroid plexus and iron is also present in scattered mesenchymal elements in the supporting tissues of the plexus.*" To further confirm this interpretation, a second analysis was performed on the same data that avoids smoothing and masking of the ventricles harboring the choroid plexuses. This analysis also showed that iron accumulation is unambiguously confined in the choroid plexuses sparing the contiguous neural tissue.

Lastly, previous chelation treatment did not significantly affect brain tissue iron content although an ongoing deferiprone was associated with lower-than-normal brain tissue iron deposits in the only three patients belonging to this small subgroup. Thus, if any, the effect of deferiprone seems to be just a transient effect as any history of previous treatment was not associated with persistently decreased iron levels. Even though further validation is needed on larger series of patients, as a whole these findings allow some interesting speculations. First, as deferiprone is the sole chelation treatment able to pass the blood-brain barrier, the latter appears to represent the main obstacle to brain iron overload in conditions of serum iron excess. Secondly, the applied MRI quantification protocol seems to be potentially sensitive to treatment-related brain iron content changes thus confirming its efficiency in detecting tissue iron levels. Finally, brain tissue homeostasis mechanisms of beta thalassemia patients seem to be able to re-establish the physiological iron content after the withdrawal of deferiprone, thus suggesting the importance of brain iron content homeostasis.

Iron overload in the brain: comparison with the available literature

The present study did not confirm previous conflicting observations regarding iron overload in the brain (Table 5). Discrepancies among studies likely derived from limited sample size of previous studies due to the disease rarity, different methodological approaches with regards to both the MRI sequences and the subsequent analysis (ROI-based on different image sections versus whole brain voxel-based analysis), patient characteristics and treatment differences (e.g. patients recruitment in different countries employing different clinical programs). The present study used (i) both a voxel-based approach in order to include every brain region and an ROI-based approach to optimize the statistical comparison, (ii) the most validated quantitative MRI protocol and image analysis pipeline that well replicated normative values and aging related trends in the literature (Callaghan et al., 2014), and (iii) an adequate sample size of TDT patients with healthy controls but also with a consistent group of NTDT patients in order to provide a more detailed evaluation of the iron overload phenomenon in the brain. According to our study, none of the previously recognized regions (but those closer to choroid plexuses) showed increased iron load (Table 5). Obviously, our data might represent the picture of patients treated according to the current guidelines from the Thalassemia International Federation (Cappellini et al., 2014). In Italy, for example, a mean hemoglobin level of 9.5 g/dL is considered a reliable target of treatment, while in other countries the level for transfusion is often set to lower levels. Dietary and environmental factors together with the regimens of chelation treatment might have also had an impact on the iron deposition in the brain leading to normal values in all regions that showed iron overload in at least one of the previous studies. As a whole, our study seems to reveal a striking sparing of the neural tissue suggesting that, with the current treatment protocols, iron overload might severely affect several organs but not the brain. Whether this result is due to the

presence of a blood brain barrier or to an efficient iron wash out system in the brain cannot be unraveled, even though preliminary data on ongoing deferiprone treatment seem to point to the role of the blood-brain barrier. Notably, the sole autoptic study provided similar findings (i.e. no iron excess in the brain but in the choroid plexuses) thus excluding the role of chelation treatments that were not available in the early sixties (Witzleben and Wyatt, 1961). In any case, it seems that imaging the brain in the search of iron overload in neurologically asymptomatic patients treated with the current guideline is not supported by our analysis at least until the forth/fifth decade of life. Future follow-up studies on ageing patients will prove if the concern about iron-related brain injury is real or simply an incorrect inference of what happens in the heart, liver and endocrine glands.

Iron overload in the brain: clinical implications

Neurological involvement in beta thalassemia has become more evident with the considerable increase of life expectancy associated to regular blood transfusion and chelation therapy. A major concern regards cognition as several cognitive fields have been shown to be variably compromised in beta-thalassemia patients (Elalfy et al., 2017). Lower cognitive performances have been attributed to disease-related chronic ischemia, to treatment side effects and to the high number of hospitalizations occurring since the very first years of life (Economou et al., 2006). Brain iron overload has been also included in the list of possible mechanisms of brain injury due to its potential neurotoxicity. Previous pioneering MRI studies have supported this hypothetical pathogenic mechanism disclosing areas of iron overload in the cortical and subcortical brain structures with a possible role in neurocognition (Metafratzi et al., 2001; Akhlaghpoor et al., 2012). The lack of evidence of neural tissue iron overload seems to curtail the causal relationship between brain iron and cognitive impairment. Nonetheless, even choroid plexus iron overload could be responsible of neurodegeneration. The production of free radicals in the cerebrospinal fluid or in tissues contiguous to regions strictly related to cognition could be a potentially dangerous pathogenic mechanism, but the lack of association between tissue iron levels and cognitive impairment in our beta-thalassemia sample and the lack of relationship between iron levels and the volume of the hippocampal formations make this hypothetical relationship rather unlikely. Therefore, according to our study, the main cause of cognitive impairment in beta-thalassemia should not be searched in iron dysmetabolism.

Limits of the study

Even though this multicenter study investigated with MRI the largest beta-thalassemia sample so far, the rarity of the disease allowed the recruitment of limited dozens of patients (47 TDT and 23 NTDT patients). The NTDT sample size might appear relatively small for firm conclusions in this subgroup. However, among beta-thalassemia patients, TDT ones typically present the most severe systemic iron overload due to blood transfusion treatment. The lack of neural tissue iron overload in the TDT subgroup points to an unlikely or scarce brain involvement in the whole disease phenotypic spectrum. Larger studies might help to refine our results even though the detection of additional areas of iron overload requiring larger series would likely have a limited clinical impact.

From a methodologic point of view, R2* might depend on other factors besides iron content, including cellularity and water content. However, there is no data about changes of these possible confounders both from histopathology and conventional MRI. In addition, although high resolution imaging makes the R2* closer to R2 measurements, R2 might outperform R2* if the iron stores are primarily ferritin, not hemosiderin, thus preventing firm conclusions from the present study. However, the fact that the histopathology of five TDT patients did not reveal significant iron increase in the brain except than in the choroid plexuses strongly support our findings (Witzleben and Wyatt, 1961). Finally, this study was conducted in a world region with treatment guidelines that are relatively conservative in terms of hemoglobin levels to be maintained and that include homogeneous indications for chelation treatment. Therefore, our results cannot be generalized to other areas of the world where transfusion regimens are regulated by lower hemoglobin levels and where chelation guidelines might be different or dependent from chelation treatment availability. Nonetheless, this study shows that, with the current beta-thalassemia treatment guidelines, there is no evidence of brain tissue iron overload but in the choroid plexuses limiting any indication in beta-thalassemia patients to follow-up brain iron content with dedicated, time consuming brain MRI protocols.

Conclusion

Even though iron poisoning is detrimental in several organs and represent a life-threatening condition in beta-thalassemia, its occurrence in the brain neural tissue might be a far more limited and circumscribed phenomenon, at least in patients undergoing conservative guidelines of treatment. In fact, brain iron overload seems to be confined in the choroid plexuses and its detection in the neural tissue (including the hippocampal formations) seems to be attributable to a blooming effect. According to study evidence, literature review and previous autoptic findings, routine monitoring of parenchymal iron overload in the brain of beta-thalassemia patients is likely not required.

Funding

This study was in part supported by the University of Salerno (project code ORSA 181 880)

Declaration of Competing Interest

None

Acknowledgments

The authors would like to thank Antonietta Canna and Andrea Gerardo Russo for their help with MRI image data acquisition and for the helpful discussions.

Supplementary materials

Supplementary material associated with this article can be found, in the online version, at doi:10.1016/j.nicl.2019.102058.

References

Taher, A.T., Weatherall, D.J., Cappellini, M.D, 2018. Thalassaemia. Lancet 391 (10116), 155–167.
Gardenghi, S., Marongiu, M.F., Ramos, P., et al., 2007. Ineffective erythropoiesis in β-thalassemia is characterized by increased iron absorption mediated by down-regulation of hepcidin and up-regulation of ferroportin. Blood 109 (11), 5027–5035.
Á, Remacha, C, Sanz, Contreras, E., et al., 2013. Guidelines on haemovigilance of post-transfusional iron overload. Blood Transfus. 11 (1), 128–139.
Hunt, J.R., Zito, C.A., Johnson, L.K., 2009. Body iron excretion by healthy men and women. Am. J. Clin. Nutr. 89 (6), 1792–1798.
Anderson, L.J., Westwood, M.A., Holden, S., et al., 2004. Myocardial iron clearance during reversal of siderotic cardiomyopathy with intravenous desferrioxamine: a prospective study using T2* cardiovascular magnetic resonance. Br. J. Haematol. 127 (3), 348–355.
Casale, M., Citarella, S., Filosa, A., et al., 2014. Endocrine function and bone disease during long-term chelation therapy with deferasirox in patients with β-thalassemia major. Am. J. Hematol. 89 (12), 1102–1106.
Aubart, M., Ou, P., Elie, C., et al., 2016. Longitudinal MRI and Ferritin monitoring of iron overload in chronically transfused and chelated children with sickle cell anemia and thalassemia major. J. Pediatr. Hematol. Oncol. 38 (7), 497–502.
Ambu, R., Crisponi, G., Sciot, R., et al., 1995. Uneven hepatic iron and phosphorus distribution in beta-thalassemia. J. Hepatol. 23 (5), 544–549.
Viprakasit, V., Ajlan, A., Aydinok, Y., et al., 2018. MRI for the diagnosis of cardiac and liver iron overload in patients with transfusion-dependent thalassemia: an algorithm

to guide clinical use when availability is limited. Am. J. Hematol.
Bozdağ, M., Bayraktaroğlu, S., Aydınok, Y., Çallı, M.C, 2017. MRI assessment of pituitary iron accumulation by using pituitary-R2 in β-thalassemia patients. Acta Radiol 028418511773009.
Hashemieh, M., Radfar, M., Azarkeivan, A., et al., 2017. Renal hemosiderosis among Iranian transfusion dependent β-thalassemia major patients. Int. J. Hematol. Stem Cell Res. 11 (2), 133–138.
Kosaryan, M., Rahimi, M., Darvishi-Khezri, H., et al., 2017. Correlation of pancreatic iron overload measured by T2*-weighted magnetic resonance imaging in diabetic patients with β -thalassemia major. Hemoglobin 41 (3), 151–156.
Langkammer, C., Krebs, N., Goessler, W., et al., 2010. Quantitative MR imaging of brain iron: a postmortem validation study. Radiology 257 (2), 455–462.
Deoni, S.C.L., Peters, T.M., Rutt, B.K, 2005. High-resolution T1 and T2 mapping of the brain in a clinically acceptable time with DESPOT1 and DESPOT2. Magn. Reson. Med. 53 (1), 237–241.
Dick, F., Taylor Tierney, A., Lutti, A., et al., 2012. In vivo functional and myeloarchitectonic mapping of human primary auditory areas. J. Neurosci. 32 (46), 16095–16105.
Helms, G., Dechent, P., 2009. Increased SNR and reduced distortions by averaging multiple gradient echo signals in 3D Flash imaging of the human brain at 3T. J. Magn. Reson. Imaging 29 (1), 198–204.
Sereno, M.I., Lutti, A., Weiskopf, N., Dick, F, 2013. Mapping the human cortical surface by combining quantitative T1 with retinotopy†. Cereb. Cortex. 23 (9), 2261–2268.
Helms, G., Dathe, H., Kallenberg, K., Dechent, P, 2008a. High-resolution maps of magnetization transfer with inherent correction for RF inhomogeneity and T 1 relaxation obtained from 3D Flash MRI. Magn. Reson. Med. 60 (6), 1396–1407.
Helms, G., Dathe, H., Dechent, P, 2008b. Quantitative Flash MRI at 3T using a rational approximation of the Ernst equation. Magn. Reson. Med. 59 (3), 667–672.
Weiskopf, N., Lutti, A., Helms, G., et al., 2011. Unified segmentation based correction of R1 brain maps for RF transmit field inhomogeneities (UNICORT). Neuroimage 54 (3), 2116–2124.
Weiskopf, N., Callaghan, M.F., Josephs, O., Lutti, A., Mohammadi, S, 2014. Estimating the apparent transverse relaxation time (R2*) from images with different contrasts (ESTATICS) reduces motion artifacts. Front. Neurosci. 8 (SEP), 1–10.
Weiskopf, N., Suckling, J., Williams, G., et al., 2013. Quantitative multi-parameter mapping of R1, PD*, MT, and R2* at 3T: a multi-center validation. Front. Neurosci. 7 (7 JUN), 1–11.
Whitaker, K.J., Vértes, P.E., Romero-Garcia, R., et al., 2016. Adolescence is associated with genomically patterned consolidation of the hubs of the human brain connectome. Proc. Natl. Acad. Sci. 113 (32), 9105–9110.
Callaghan, M.F., Freund, P., Draganski, B., et al., 2014. Widespread age-related differences in the human brain microstructure revealed by quantitative magnetic resonance imaging. Neurobiol. Aging 35 (8), 1862–1872.
Tartaglione, I., Russo, C., Elefante, A., et al., 2019a. No evidence of increased cerebrovascular involvement in adult neurologically-asymptomatic β-Thalassaemia. A multicentre multimodal magnetic resonance study. Br. J. Haematol. 5. https://doi.org/10.1111/bjh.15834.
Tartaglione, I., Manara, R., Caiazza, M., et al., 2019b. Brain functional impairment in beta-thalassemia: the cognitive profile in Italian neurologically asymptomatic adult patients and review of the literature. Br. J. Haematol. in press.
Weiskopf, N., Helms, G., 2008. Multi-parameter mapping of the human brain at 1 mm resolution in less than 20 min. Proc. Int. Soc. Magn. Reson. Med. 16, 2240–2241.
Draganski, B., Ashburner, J., Hutton, C., et al., 2011. Regional specificity of MRI contrast parameter changes in normal ageing revealed by voxel-based quantification (VBQ). Neuroimage 55 (4), 1423–1434.
Ashburner, J., Friston, K.J, 2005. Unified segmentation. Neuroimage 26 (3), 839–851.
Ashburner, J, 2007. A fast diffeomorphic image registration algorithm. Neuroimage 38 (1), 95–113.
Postelnicu, G., Zollei, L., Fischl, B, 2009. Combined volumetric and surface registration. IEEE Trans. Med. Imaging 28 (4), 508–522.
Canna, A., Ponticorvo, S., Russo, A.G., et al., 2018. A group-level comparison of volumetric and combined volumetric-surface normalization for whole brain analyses of myelin and iron maps. Magn. Reson. Imaging 54 (August), 225–240.
Maldjian, J.A., Laurienti, P.J., Kraft, R.A., Burdette, J.H, 2003. An automated method for neuroanatomic and cytoarchitectonic atlas-based interrogation of fMRI data sets. Neuroimage 19 (3), 1233–1239.
Gillen, K.M., Mubarak, M., Nguyen, T.D., Pitt, D, 2018. Significance and in vivo detection of iron-laden microglia in white matter multiple sclerosis lesions. Front. Immunol. 9 (FEB), 1–8.
Kuchcinski, G., Munsch, F., Lopes, R., et al., 2017. Thalamic alterations remote to infarct appear as focal iron accumulation and impact clinical outcome. Brain 140 (7), 1932–1946.
Di Meo, I., Tiranti, V, 2018. Classification and molecular pathogenesis of NBIA syndromes. Eur. J. Paediatr. Neurol. 22 (2), 272–284.
Ji, X., Cui, N., Liu, J, 2017. Neurocognitive function is associated with serum iron status in early adolescents. Biol. Res. Nurs. 19 (3), 269–277.
Elalfy, M.S., Aly, R.H., Azzam, H., et al., 2017. Neurocognitive dysfunction in children with β thalassemia major: psychometric, neurophysiologic and radiologic evaluation. Hematology 22 (10), 617–622.
Monastero, R., Monastero, G., Ciaccio, C., Padovani, A., Camarda, R, 2000. Cognitive deficits in beta-thalassemia major. Acta Neurol. Scand. 102 (3), 162–168.
Metafratzi, Z., Argyropoulou, M.I., Kiortsis, D.N., et al., 2001. T2 relaxation rate of basal ganglia and cortex in patients with b-thalassaemia major. Br. J. Radiol. 74, 407–410.
Akhlaghpoor, S., Ghahari, A., Morteza, A., et al., 2012. Quantitative T2* magnetic resonance imaging for evaluation of iron deposition in the brain of β-thalassemia patients. Clin. Neuroradiol. 22 (3), 211–217.
Qiu D., Chan G.C., Chu J., et al. MR quantitative susceptibility imaging for the evaluation of iron loading in the brains of patients with ^{NL} -Thalassemia major. 2014;1085–1090.
Hasiloglu, Z.I., Asik, M., Ure, E., et al., 2017. The utility of susceptibility-weighted imaging to evaluate the extent of iron accumulation in the choroid plexus of patients with b -thalassaemia. Clin. Radiol. 1–7.
Pirpamer, L., Hofer, E., Gesierich, B., et al., 2016. Determinants of iron accumulation in the normal aging brain. Neurobiol. Aging 149–155.
Aquino, D., Bizzi, A., Grisoli, M., et al., 2009. Age-related iron deposition in the basal ganglia: quantitative analysis in healthy subjects. Radiology 165–172.
Witzleben, C.L., Wyatt, J.P., 1961. The effect of long survival on the pathology of thalassæmia major. J. Pathol. Bacteriol. 82 (1), 1–12.
Cappellini M.D.; Cohen A.; Porter J.; Taher A.; Viprakasit V. Guidelines for the management of transfusion dependent thalassemia (TDT). 2014.
Economou, M., Zafeiriou, D.I., Kontopoulos, E., et al., 2006. Neurophysiologic and intellectual evaluation of beta-thalassemia patients. Brain Dev. 28 (1), 14–18.